THE JOURNAL OF PHYSICAL CHEMISTRY C

Article

Cite This: J. Phys. Chem. C 2018, 122, 7179−7186

pubs.acs.org/JPCC

Investigation on the Wetting Behavior of 3C-SiC Surfaces: Theory and Modeling

C. Ulises Gonzalez-Valle,[†] Satish Kumar,[‡] and Bladimir Ramos-Alvarado*[,†]

[†]Department of Mechanical and Nuclear Engineering, The Pennsylvania State University, University Park, Pennsylvania 16802, United States

[‡]The George W. Woodruff School of Mechanical Engineering, Georgia Institute of Technology, Atlanta, Georgia 30332, United States

ABSTRACT: Silicon carbide (SiC) is a promising material for high-power and high-frequency electronics due to its wide band gap, large breakdown field, and high thermal conductivity. Several applications of micro- and nanoelectronics are found in aqueous environments; thus, it is important to understand the atomic-scale interactions between SiC and water, as these interactions govern the transport processes at solid−liquid interfaces. In an effort to characterize the solid−liquid interactions, the wetting behavior of 3C-SiC was numerically investigated. The wettability of two crystallographic planes ((100) and (111)) was characterized, allowing to have silicon or carbon terminations. It was found that the crystallographic planes as well as the atomic surface terminations play an important role in the wetting behavior of 3C-SiC. Higher hydrophilicity was observed for the Si-terminated surfaces as well as for the SiC(111) crystallographic plane. A combination of a mean-field model of wettability and an analysis of the interfacial liquid structuring led to explain the wetting behavior of the different crystallographic planes (silicon- or carbon-terminated). These numerical and theoretical findings underscore the importance of proper modeling strategies when using wetting behavior as the framework for the modeling of interfaces.

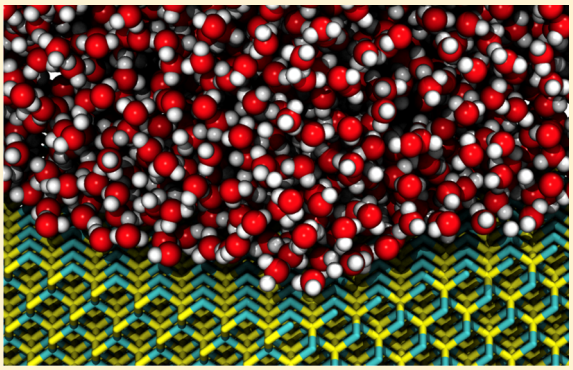

1. INTRODUCTION

The wetting behavior of solid surfaces and the understanding of its governing mechanisms are topics of vast interest for the scientific community. The phenomena involved during wetting are of particular importance due to the large number of technological processes, where wetting dictates the behavior of chemical reactions,[1] heat,[2] momentum transfer,[3] evaporation,[4] etc. Molecular-level simulations offer a physically sound platform for the investigation of the underlying nature of the wetting phenomenon; particularly, classical molecular dynamics (MD) simulations have been extensively used owing to the availability of faster force fields in comparison to the first-principles methods, such as ab initio density functional theory simulations.

Graphitic carbon surfaces offer a popular test bench for numerical and theoretical investigations of wettability. It is common to find literature using graphene or graphite to test new modeling techniques,[5] theories,[6] postprocessing methods,[7] etc. Werder et al.[8] conducted one of the cornerstone investigations in the field of MD simulations of wettability. While conducting droplet wettability simulations of graphitic carbon surfaces, they observed a linear relationship between the contact angle and the water monomer binding energy on graphite. Werder et al.[8] proposed to use this relation to calibrate the water−carbon interaction potential while matching the simulation results in the macroscopic limit with the experimental contact angle of graphite. Taherian et al.[9] investigated the wettability of graphitic carbon surfaces from single-layer graphene to bulk graphite using MD simulations. A correlation between the interaction potential of the water molecules and the work of adhesion was observed. Additionally, the interfacial energy and entropy changes, as well as the water−solid binding energy were used to explain the transition from two-dimensional material (graphene) wetting behavior to bulk (graphite) wetting properties. More recently, Leroy et al.[10] have investigated the wetting characteristics of graphene wetted by different water models and found that the work of adhesion depends weakly on the water model for a given set of force-field parameters. The contact angle was calculated using the same water models, and the observed trends were explained in terms of the properties of the water models, namely, the surface tension. Thus, Leroy et al.[11] suggested to optimize the force potentials for water on carbon surfaces such that the experimental work of adhesion is reproduced in MD simulations.

Unlike graphitic surfaces, the wetting behavior of metals, such as gold and copper,[12,13] and semiconductors, like silicon[14−16] (Si), has received less attention from the modeling

Received: December 13, 2017
Revised: February 12, 2018
Published: March 9, 2018

DOI: 10.1021/acs.jpcc.7b12271
J. Phys. Chem. C 2018, 122, 7179−7186

and theoretical points of view. This is mainly due to the challenges posed by the instantaneous growth of oxide layers when these materials are exposed to the environment. Likewise, most of the investigations are focused on pure crystalline solids, but there is a scarcity of information for compound materials. Ohler and Langel[17] conducted an MD investigation of the wetting behavior of titanium dioxide (TiO_2). They found that the direct contact between the solid and the bulk liquid does not determine the macroscopic contact angle of water on TiO_2; conversely, the macroscopic contact angle was found to be dependent on a thin water film, which was formed over the solid phase. Köppen and Langel[18] observed that water located at 7 Å from the TiO_2 surface is highly ordered, but water molecules at a distance of 10 Å or farther from the surface are randomly oriented; hence, the orientation produced in the surroundings of the solid phase will influence the wettability observed on the substrate. Govin-Rajan et al.[19] reported an investigation on the wettability of molybdenum disulfide (MoS_2) surfaces. It was suggested that the partially ionic bonds present in MoS_2 would prompt interfacial solid−liquid interactions dominated by electrostatic forces, unlike materials with covalent bonds like graphene. The results indicated that electrostatic forces play a negligible role in the solid−liquid interactions on the MoS_2 basal plane, contributing less than 0.52% of the total interaction energy; the contact angle was found to depend solely on the solid−liquid dispersive forces (interaction energy and entropic contributions).

Silicon carbide (SiC) is a promising material for high-power and high-frequency applications due to its wide band gap, large breakdown field, and large thermal conductivity. It has been considered as a material for the next-generation high-power and high-temperature devices.[20] Additionally, SiC is one of the best biocompatible materials, making it especially useful in cardiovascular, blood-contacting implants, and other biomedical devices.[21] Oliveros et al.[22] compared the water contact angles of 3C-SiC(100) before and after surface modification with 3-aminopropyltriethoxysilane. They found contact angles of 16 ± 3° for SiC before and 61 ± 1° after the procedure. Ma et al.[23] studied the wetting behavior of laser-modified SiC surfaces. The results showed that the microsquare convex structures changed the wetting behavior of SiC surfaces, increasing the contact angle after the laser treatment. The contact angle was found to increase from 100.2 to 119°, increasing the roughness from 1 to 3 μm, whereas the untextured surface showed a contact angle of 89.8°. As it can be observed, several experimental analyses showed different values for bare SiC surfaces starting from highly hydrophilic (~16°) to hydrophobic conditions (~90°).

3C-SiC is the only cubic polytype known for SiC. All of the natural polytypes that are known have the same atomic composition, but their electrical properties differ. 3C-SiC presents the highest electron mobility and saturation drift velocity due to its cubic nature.[24,25] 3C-SiC is the only polytype that can be heteroepitaxially grown on Si subtracts. This is important for microelectromechanical systems (MEMS) fabrication because large-area Si substrates are available in the market.[24] Following the advantages of this SiC polytype in MEMS fabrication, wettability plays a significant role in thin-film-based biosensor applications. Thus, a proper understanding of the wetting behavior of SiC surfaces can promote further development in the fabrication and implementation of this material in thin-film applications. In this investigation, a wide range of wetting conditions were numerically simulated using MD simulations. An analytical model was developed based on the mean-field (MF) theory to establish a link between microscopic properties and macroscopic observable effects of wettability. Wettability anisotropy of different SiC planes was observed, and a combination of theory, provided by our MF model, and characterizations of the interfacial liquid structure helped to explain such observations. These findings demonstrate that using wetting behavior for the modeling of interfacial interactions must be taken into account with caution, as not only solid−liquid affinity but also the structure of the wetted surface play a significant role in the wetting process.

2. METHODOLOGY

2.1. Analytical Model of Wettability for Compound Materials. The main characteristic of an MF model is the reduction of a multibody problem to a single-body problem. Clearly, the solid−liquid interactions at an interface are evidently a multibody problem that can be simplified using MF theory. In addition to an MF approach, the following assumptions helped to develop a 3C-SiC wettability model: (i) the solid−liquid interactions are predominantly dispersive; (ii) the liquid−solid interactions are modeled using a Lennard-Jones (LJ) potential (see eq 1); and (iii) the solid−liquid interactions for Si and C are additive. The LJ potential was used to model the solid−liquid interactions as

$$V_{ij} = 4\varepsilon_{ij}\left[\left(\frac{\sigma_{ij}}{r}\right)^{12} - \left(\frac{\sigma_{ij}}{r}\right)^{6}\right] \tag{1}$$

where r is the distance between two particles, and ε_{ij} and σ_{ij} are the LJ parameters for the ij pair of solid−liquid atoms. Water has two atom types, H and O, and the hydrogen−solid interactions were neglected; thus, the ε_{ij} and σ_{ij} coefficients are defined for the oxygen−silicon and oxygen−carbon interactions. Discrete pairwise interactions are made continuous if an infinite x−y plane of the solid substrate is considered and has a constant atomic density per unit area ρ_s. Additionally, if an infinite potential cutoff is assumed, the interaction potential for a water molecule over the atomic plane is

$$w(z) = 4\pi\rho_s\varepsilon\sigma^2\left(\frac{\sigma^{10}}{5z^{10}} - \frac{\sigma^4}{2z^4}\right) \tag{2}$$

where z is the distance between a water molecule and the solid plane. Recalling assumption (iii), the total single-particle potential can be obtained by adding the contributions of $w(z)$ from N atomic layers. As it can be observed in Figure 1, 3C-SiC presents intercalated Si and C layers, and this effect is considered in

$$w_N(z) = 4\pi\sum_{(i)=1}^{n}\sum_{k_{(i)}}^{N_{(i)}-1}\left\{\begin{array}{l}\rho_{s(i)}\varepsilon_{(i)O}\sigma_{(i)O}^2\left[\dfrac{\sigma_{(i)O}^{10}}{5(z+\delta_{\mathrm{off}(i)}+k_{(i)}h_{(i)})^{10}}\right]\\ -\rho_{s(i)}\varepsilon_{(i)O}\sigma_{(i)O}^2\left[\dfrac{\sigma_{(i)O}^{4}}{2(z+\delta_{\mathrm{off}(i)}+k_{(i)}h_{(i)})^{4}}\right]\end{array}\right\} \tag{3}$$

The index (i) indicates the material (i = 1 for Si and i = 2 for C), n is the number of materials in the solid, and $\delta_{\mathrm{off}(i)}$ is an offset distance, which specifies the termination of the surface. For example, $\delta_{\mathrm{off(Si)}} = 0$ if the substrate is Si-terminated and $h_{(i)}$ is defined as the interlayer distance between atomic planes of the same material. The spatial parameters used in eq 3 are described in Figure 1 as h_0, h_1, and h_2. These parameters are

DOI: 10.1021/acs.jpcc.7b12271
J. Phys. Chem. C 2018, 122, 7179−7186

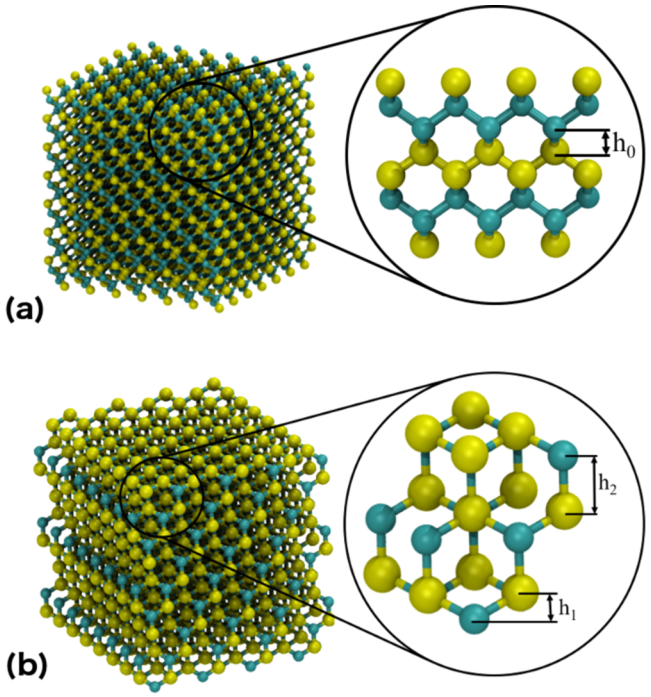

Figure 1. Silicon carbide structures (a) SiC(100) and (b) SiC(111). The yellow spheres represent Si atoms, and the teal spheres represent C atoms.

defined in terms of the SiC lattice constant (a_{SiC} = 4.3596 Å) as $h_0 = a_{SiC}/4$, $h_1 = a_{SiC}\sqrt{3}/12$, and $h_2 = a_{SiC}\sqrt{3}/4$. A similar approach can be applied to any composite material as long as the different components are intercalated and homogeneously distributed in each atomic layer.

According to Shih et al.,[26] the work of adhesion of graphene-coated surfaces can be computed by adding the individual contributions of the solid atoms in the coated structure. It is plausible to apply the same principle for the calculation of $w(z)$ in compounds by considering the individual contribution of each material to the total work of adhesion. These contributions have been already considered in eq 3. The total work can be computed as shown in eq 4; this is the Young–Dupre equation, which describes the contact angle on a surface in terms of the work of adhesion[27]

$$W_A = \frac{1}{A}(\Delta U_{WS} - T\Delta S_{WS}) = \gamma_{LV}(1 + \cos\theta) \quad (4)$$

where W_A represents the work of adhesion, ΔU_{WS} is the total solid–liquid interaction energy per unit area, T is the absolute temperature of the system, $-\Delta S_{WS}$ is the interfacial entropy due the structural bias imposed on the water molecules by a nonrepulsive external potential from the solid substrate,[28,29] γ_{lv} is the surface tension of water, and θ is the contact angle. W_A can be considered as the amount of energy that is needed to separate a fluid from a solid per unit area; it is the reversible work required to create and destroy interfaces. In this model, the $-\Delta S_{WS}$ term was not considered explicitly; however, the model developed herein is optimized against MD simulations using a fitting parameter (η), which helps in establishing the connection between microscopic and macroscopic parameters. The W_A can be computed as

$$W_A = -\int_0^\infty \rho_L(z) w_N(z)\, dz \quad (5)$$

where $\rho_L(z)$ is the number density normal to the wetted plane. Several $\rho_L(z)$ distributions have been previously used.[15,27,30] The modified Boltzmann distribution proposed by Ramos-Alvarado et al.[15] closely describes the concentration of liquid particles near carbon surfaces and other wetting behavior reported from MD simulations.[15] This model is given by

$$\rho_L(z) = \rho_{L,0} \exp\left[\frac{-w_N(z)}{\eta k_B T}\right] \quad (6)$$

where $\rho_{L,0}$ is the bulk density of the liquid, k_B is the Boltzmann constant, T is the absolute temperature, and η is the only fitting parameter of the model. The parameter η is of utmost importance as it accounts interfacial effects not explicitly considered. The role played by η is adjusting the concentration of liquid particles at the interface, thus accounting for $-\Delta S_{WS}$ and deviations from the representation of $w_N(z)$ by a continuous function to eventually obtain the ΔU_{WS} and ΔU_{WS} contributions to W_A.

The wettability model developed herein (eqs 1–6) contains a fitting parameter, which can be calibrated using a single MD-data point. This model was not designed to substitute MD simulations of wettability, but to establish a link between the microscopic properties of the wetted surfaces with macroscopic observables, such as W_A and θ. Additionally, it adds a simplification to a known problem, i.e., having a realistic model of ΔS_{WS} that can be used for a wide range of wetting conditions (see ref 30 and the Supporting Information of ref 15).

2.2. Molecular Dynamics Model. The wetting behavior of SiC surfaces was characterized by MD simulations of cylindrical water droplets[5] to obtain the static contact angle. The SPC/E[31] water model was used due to its simplicity, low computational cost, and the wide spread utilization of this model, which allows for comparison with previous investigations. The SHAKE[32] algorithm was implemented to enforce the rigidity of the water molecule, and an accuracy of 1×10^{-5} was used for the PPPM[33] algorithm implemented to treat the Coulombic interactions in the water model. Similar to the MF model of wettability developed in the previous section, only the oxygen–solid interaction was considered.[8,15]

Modeling the solid–liquid interactions in a compound is more challenging that in elemental surfaces. There are at least two types of solid atoms interacting with the liquid particles, and questions arise on the proper approach. We have assumed that the C–O interactions could be represented by the LJ parameters σ_{C-O} = 3.19 Å and ε_{C-O} = 0.005 eV, which were optimized to obtain a contact angle of 64° for water over a pristine graphitic surface.[15,34] The Si–O interactions have not been extensively characterized in the literature; likewise, the contact angle of Si is not consistent among experimental reports; therefore, the energy parameters of the LJ potential for Si–O (ε_{Si-O}) was varied to account for a wide range of wetting conditions. This was done from 0.0065 to 0.0243 eV and from 0.0055 to 0.0212 eV for SiC(100) and SiC(111), respectively, maintaining σ_{Si-O} = 2.63 Å. For all of the cases, the cutoff radius was 15 Å. The number of molecules in the water droplets was varied from 2500 to 8500 to verify size effects. Testing the effectiveness of this modeling approach for the wettability of compound materials was one of the objectives of the current investigation. The assessment of this assumption will be presented in the following section. The solid substrate was kept fixed by not solving its dynamics. It has been proven that a

DOI: 10.1021/acs.jpcc.7b12271
J. Phys. Chem. C 2018, 122, 7179–7186

flexible solid model has a negligible effect on the contact angle computations.[8,15,16] Periodic boundary conditions were set in the three directions of the computation box. The y-direction length of the system was 30.61 Å for SiC(100) and 31.48 Å for SiC(111), and the length in the x-direction was varied from 250 to 350 Å depending on the size of the droplet. The z-direction length was large enough to eliminate any boundary influence in the analysis. The open-source code LAMMPS[35] was used for the MD simulations alongside with VMD[36] for visualization purposes. The time step used for the simulations was 1 fs. To avert any random drifting, the center of mass of the water droplet was reset to its original position (x and y) each time step and the neighbor lists were also updated every time step.

The simulation process included the following steps: (i) an energy minimization was performed to remove any potential energy excesses caused by the initial configuration; (ii) the system was equilibrated at 298 K applying a Nosé−Hoover[37,38] thermostat with a time constant of 0.1 ps during 0.75 ns; (iii) the Nosé−Hoover thermostat was removed and a microcanonical integrator was used for 1 ns under purely Newtonian dynamics, as a check of a proper equilibration; (iv) the production run was performed collecting snapshots of the water molecules every 0.5 ps for 5 ns under the microcanonical ensemble. Once the results from the MD simulations were obtained, the shape of the water droplets was determined by time-averaging the density contours. The averaging was performed every 10 snapshots, considering the accumulation of data over time. The MRPM method proposed by Ramos-Alvarado et al.[15] was followed to improve the quality and steadiness of the performed computations and finally to obtain a reliable calculation of the contact angle.

3. RESULTS AND DISCUSSION

3.1. Contact Angle Calculations. Four SiC surfaces were analyzed, namely, two crystallographic planes with two different atomic terminations each. The MD simulations were performed following the method previously described. A single MD simulation data point was used to find the fitting parameter η for each crystalline plane (see eq 6). The values of η were 3.1 and 2.8 for SiC(100) and SiC(111), respectively. It is noteworthy that η = 2.9 produced an accurate description for both cases. Figure 2 illustrates the good match between numerical and analytical calculations of the contact angle after the optimization of the MF model (eqs 1−6).

Figure 3 depicts the individual characterization of the different crystallographic planes having different atomic terminations. As it can be observed for both crystallographic planes, Si-terminated surfaces are more hydrophilic than C-terminated surfaces. For small values of ϵ_{Si-O} (hydrophobic conditions), a difference of ∼15° was observed between Si- and C-terminated surfaces. This difference becomes more substantial for more hydrophilic conditions, especially for the SiC(111) crystallographic plane, where a contact angle difference of ∼100° was observed between both terminations, ∼6.7 times larger than the observed difference presented under hydrophobic conditions. It was found that for similar ϵ_{Si-O} the computed contact angle differed for different planes and terminations. It is noteworthy that this behavior was captured by the MF model reported in eqs 1−6, where the SiC structure anisotropy prompted a different wetting response between crystalline planes, as indicated in Figure 3.

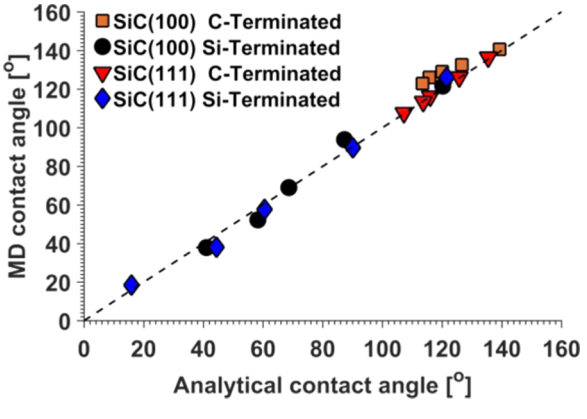

Figure 2. Comparison between MD and analytical results.

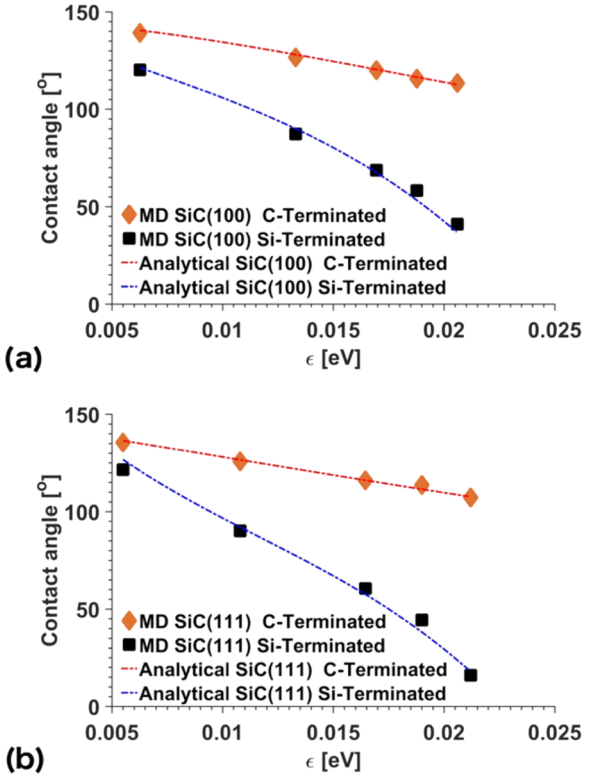

Figure 3. Theoretical and numerical contact angle calculations as a function of ϵ_{Si-O} for (a) SiC(100) and (b) SiC(111) crystallographic planes.

A classical molecular model of wettability of a solid made of one single type of element consists in finding a proper force-field potential to represent the solid−liquid interactions. On the basis of this idea, the molecular-level modeling of a compound presents additional challenges and questions arise, i.e., is an optimization of the force potentials for the different solid−liquid pairs required such that the potentials are derived for the compound as a whole, or do previously characterized solid−liquid force potentials of the elements forming the compound suffice? The wettability of carbon surfaces has been extensively studied via molecular modeling, and the optimization of the force fields has been previously established. Therefore, the water−carbon interactions of the carbon atoms in SiC were such that a contact angle of ∼64° was obtained in the macroscopic limit of a molecular-level simulation of pure graphite. As indicated, the water−carbon force field was

DOI: 10.1021/acs.jpcc.7b12271
J. Phys. Chem. C 2018, 122, 7179−7186

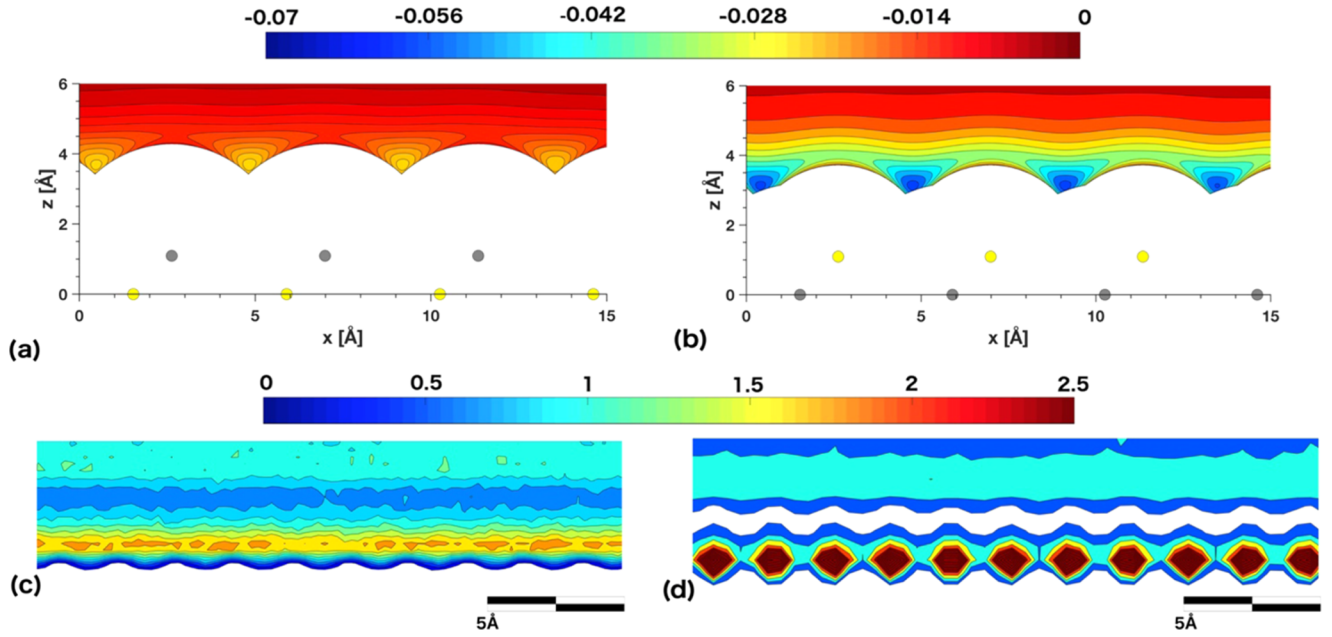

Figure 4. Solid−water interface observation on the SiC(100) crystallographic plane. Solid−liquid interacting potential on (a) C-terminated and (b) Si-terminated surfaces and density contours at the interface of (c) C-terminated and (d) Si-terminated surfaces. The interacting potential scale is in eV, and density contours scale is in g/cm^3.

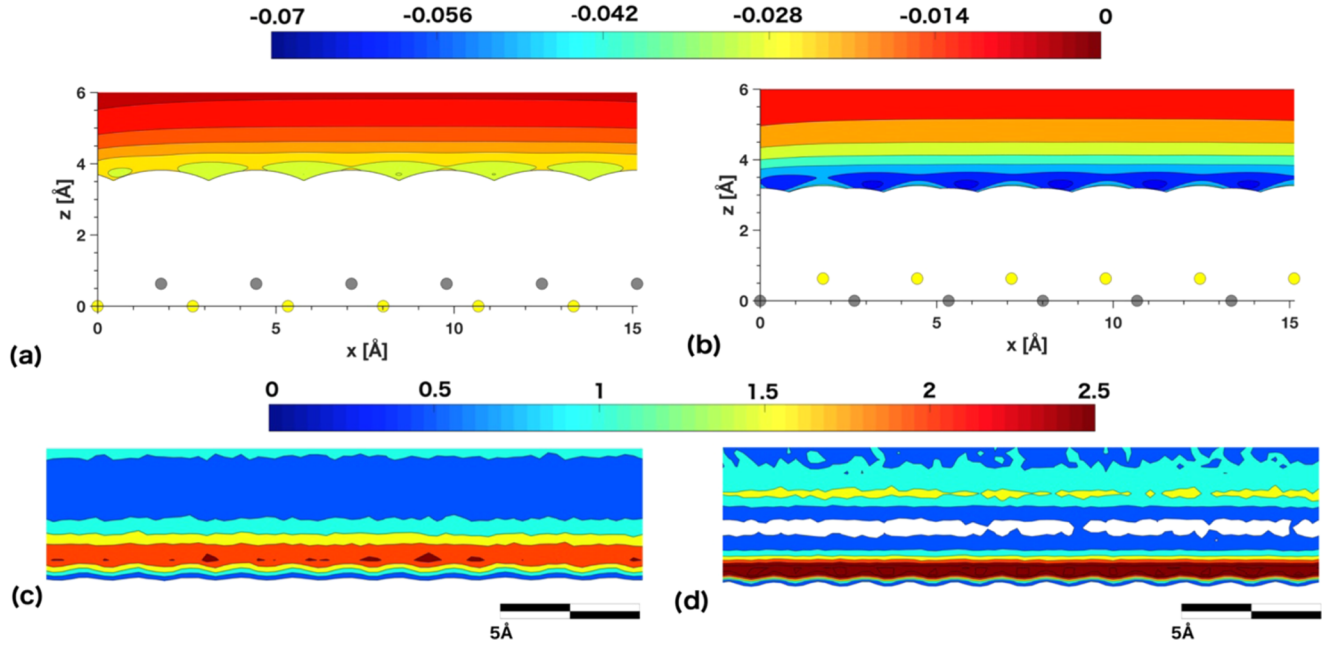

Figure 5. Solid−water interface observation on the SiC(111) crystallographic plane. Solid−liquid interacting potential on (a) C-terminated and (b) Si-terminated surfaces and density contours at the interface of (c) C-terminated and (d) Si-terminated surfaces. The interacting potential scale is in eV, and density contours scale is in g/cm^3.

optimized for a given solid structure, and this idea will be discussed further later on.

According to the results depicted in Figure 3, when the wetted surface is Si-terminated, a wide range of contact angles is observed, which includes the previously reported ∼16 and ∼90°.[22,23] Conversely, when the wetted surface is C-terminated, the range of contact angles observed is drastically reduced. The optimized length parameter for the carbon−water interactions is σ_{C-O} = 3.19 Å, which is directly proportional to the equilibrium distance between the liquid and solid phases.[15] The equilibrium distance generated by the short-ranged repulsive forces between C and water and the distance between Si and C atoms in the first atomic layer of SiC add up to increase the effective distance between Si and water; consequently, the contribution of the underlying Si atoms to the total solid−liquid interactions is minimum. In the following section, a more detailed analysis of the interfacial liquid structuring is presented. The idea of the interfacial liquid structure and interaction energy introduced here will be elaborated further in an effort to explain the interaction force fields and crystallographic topography effects on the anisotropic behavior of wettability in SiC surfaces.

DOI: 10.1021/acs.jpcc.7b12271
J. Phys. Chem. C 2018, 122, 7179−7186

Figure 3 reports anisotropy of wettability for all of the surface terminations. This crystallographic anisotropy effect on the wettability has been observed before in silicon[14,15] and Iβ cellulose[39] surfaces. In terms of the anisotropic behavior of wettability of different crystal planes, Grzelak et al.[40] reported a comprehensive analysis of this phenomenon and observed wetting anisotropy in FCC, BCC, and SC crystals (amorphous structures were also investigated). They used simple LJ systems of solids interacting with atomic liquids. In ref 41, the authors observed a close relationship between $\cos(\theta)$ and ρ_s for different solid structures and crystal planes. Linear fits of the $\cos(\theta)-\rho_s$ data were obtained, and R^2 values ranging from 0.5 to 0.77 were reported. A physically sound explanation for looking into this relationship was given, in addition to references to previous works; however, they did not support their findings with any mathematical model. In Section 3.3, we will explain the anisotropic behavior of wettability of SiC using our mean-field model with supporting data obtained from MD simulations. Additionally, and in an effort to better understand such a phenomenon, the characteristics of the interfacial liquid structure and force potential are reported in this section.

Figure 4 depicts the combined effect of the crystalline structure and the surface termination on the solid−liquid interaction potential and liquid structuring at the interface of the SiC(100) plane. For each surface, the uppermost layer termination was different (C- or Si-terminated) and the wetting condition is the most hydrophilic one, according to Figure 3. The energy contours depicted in Figures 4a,b show a rather rough interfacial energy landscape, over which the liquid particles settle. Figure 4c,d depicts the density contours at the SiC(100) interface, where the influence of the potential energy topography can be observed. Figure 4c denotes a wiggly interfacial density, which corresponds to the rough energy contours generated by the C-terminated surface. Figure 4d illustrates the creation of highly structured liquid regions at the Si-terminated SiC(100) interface. These regions are generated over surfaces with high solid−liquid affinity, and the arrangement is mainly governed by the atomistic array of the solid surface.[42] The organized interfacial structure is only observed for the Si-terminated interface because of the larger value of the solid−liquid equilibrium distance presented for the C-terminated surface. The equilibrium distance is proportional to the interaction potential length parameter, σ_{ij}; thus, the solid−liquid affinity is stronger for Si-terminated surfaces, which explains the deeper potential energy wells in Figure 4b in comparison to those in Figure 4a, hence explaining the interfacial liquid structuring.

The interaction energy and density contours for the SiC(111) interface are depicted in Figure 5. The crystallographic plane (111) is known for being the most atomically dense in a cubic diamond lattice; thus, it was expected to observe a flatter energy landscape for this solid−liquid interface compared to the SiC(100) plane. The compactness of the structure promotes the formation of a flat energy potential topography by the overlapping of the force fields generated by the solid−liquid interactions, as observed in Figure 4a. As in the (100) plane, the C-terminated interface presents a larger equilibrium distance for the liquid particles than the Si-terminated surface. Again, having large solid−liquid equilibrium distances causes to have lower interfacial interaction energies and lower concentration of liquid particles at the interface (see Figure 5c,d). The smother density contours depicted in Figure 5c,d also reflect the flatter interaction energy landscape generated by the denser SiC(111) plane.

The large repulsive zones presented for the C-terminated surfaces (Figures 4 and 5), which can also be considered as larger equilibrium distances between solid and liquid atoms, help to explain the notable differences in the wetting behavior of C- and Si-terminated surfaces for the different SiC planes. In other words, C-terminated surfaces induce larger equilibrium distances than Si-terminated surfaces; therefore, the total solid−liquid interaction decreases, as this is a function of distance between particles, and the total energy of interaction is proportional to the work of adhesion. Additionally, the difference in planar density for the (100) and (111) planes helps to explain the anisotropic behavior of wettability, a feature that the MF model of wettability presented in eqs 1−6 clearly demonstrates, as the work of adhesion is proportional to ρ_s, where ρ_s is greater for the (111) than for the (100) plane.

3.2. Interfacial Energy and Liquid Structure. Figure 6 depicts the density profiles along the droplet center-line in the

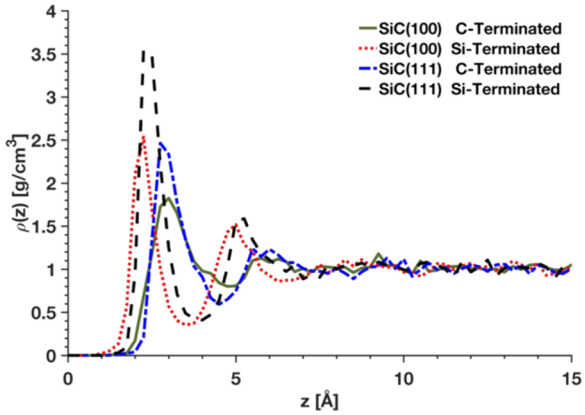

Figure 6. Droplet center-line density profiles along the z-direction for different termination under hydrophobic conditions.

z-direction (through-plane direction) for the hydrophilic conditions depicted in Figures 4 and 5. If the solid−liquid equilibrium distance is defined at the position of the first density peak, it is found that the density peaks are located at $z_{eq} \sim 3$ Å and $z_{eq} \sim 2.25$ Å for C- and Si-terminated surfaces, respectively, and such distances match the equilibrium density predictions from Figures 4 and 5. Hashibon et al.[41] presented a model to calculate the decay of density peaks based on the computed density profiles from the MD simulations as

$$\rho(z) = a \exp(\kappa z) + b \tag{7}$$

where a is a normalization factor, b is a fitting term, which considers the background or atomic distribution of the substrate, and $\kappa = 1/\xi$, where ξ is proportional to the interfacial correlation length. In this investigation, ξ is defined as an order factor (thus, κ will be a "disorder" factor). Equation 7 was used to fit the data obtained from the MD results illustrated in Figure 6 and the density decay was computed. This process was done for the four different surfaces at the hydrophilic and hydrophobic limits. The values of a, κ, and b are presented in Table 1. It is observed that the values of a and κ are larger for Si-terminated surfaces and SiC(111) crystallographic plane. According to Hashibon et al.,[41] κ gives an estimation of the penetration of the interfacial disorder into the bulk of the liquid. As it can be observed in Figure 6 and corroborated in

DOI: 10.1021/acs.jpcc.7b12271
J. Phys. Chem. C 2018, 122, 7179−7186

Table 1. Fitting Parameters of the Density Decay

surface type	a (g/cm^3)	b (g/cm^3)	κ (1/Å)
Hydrophobic Condition			
SiC(100) C-terminated	2.539	1	−5.577
SiC(100) Si-terminated	3.741	1	−7.391
SiC(111) C-terminated	4.062	1	−6.144
SiC(111) Si-terminated	7.882	1	−7.603
Hydrophilic Condition			
SiC(100) C-terminated	3.741	1	−4.625
SiC(100) Si-terminated	10.85	1	−7.467
SiC(111) C-terminated	4.317	1	−7.391
SiC(111) Si-terminated	11.54	1	−9.01

Table 1, the Si-terminated surfaces produce liquid layering that extends deeper into the bulk of the liquid. Therefore, increasing the total number of particles contributing to the solid−liquid interactions provides a secondary argument to support the difference in wettability between SiC surfaces with different atomic terminations reported in Figure 3.

3.3. Contact Angle Reconciliation. On the basis of the arguments presented so far that involved the consideration of the nanoscale topography of the wetted planes on the contact angle calculations, a reconciliation of the different wetting conditions for the analyzed surface was proposed using our MF model of wettability. Figure 7 presents the wetting behavior of different surfaces as a function of the solid−liquid interaction energy per unit area or $\epsilon\rho_s$. The expression $1 + \cos(\theta)$ is directly proportional to the work of adhesion as it can be observed from eqs 4−6; thus, a reconciliation considering $\epsilon\rho_s$ was expected and verified in Figure 7. The use of $\epsilon\rho_s$ reconciles the two crystallographic planes wetting behavior by including the energy contribution of the different underlying wetted planes in the total solid−liquid interactions.

If the lines depicted in Figure 3 are extrapolated to 0 eV, meaning that only the carbon atoms interact with water, the resulting contact angle is ∼130°. For the same carbon−water force-field parameters, the contact angle on graphene is ∼75°. Clearly, it is unexpected to observe the contact angle of graphene on C-terminated SiC when the Si−water interaction is null. Thus, not only the type of atom but also the crystallography of the structure must be considered when optimizing solid−liquid force-field potentials via wettability simulations. The parameter $\epsilon\rho_s$ captures not only the energy of interaction but also the topography of the wetted plane for the same atomic termination. However, this parameter does not reconcile the wetting behavior of the different terminations. The parameter $\epsilon\rho_s$ was previously reported by Ramos-Alvarado et al.[43] to reconcile the wettability of different Si planes. More recently, Leroy et al.[11] have suggested that W_A is a more convenient parameter for the optimization of solid−liquid force-field potentials. As it can be seen from combining eqs 4−6, $W_A \sim \epsilon\rho_s$. On the basis of the results reported in ref 11, $W_A \sim \epsilon\rho_s$ can be used to explain wettability simulations when the σ parameter of the solid−liquid interactions does not differ significantly between different systems, but as indicated in Figure 7, when σ is different enough that it affects the solid−liquid equilibrium distances, the reconciliation breaks down. This is a continuous area of research in our group and we encourage others to contribute.

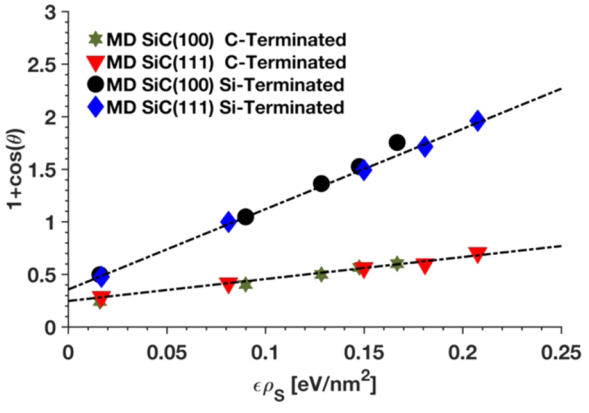

Figure 7. Reconciliation of the contact angle for different surface terminations as a function of the solid−liquid interaction energy per unit area.

4. CONCLUSIONS

In this investigation, the wetting behavior of 3C-SiC was numerically investigated and characterized via MD simulations. Four different surfaces were studied, two crystallographic planes (100 and 111) and two different surface terminations (Si and C). An analytical model was developed based on the MF theory and optimized with the results obtained from the numerical analysis. The analytical model was found to describe the wetting behavior of SiC, and the MF theory was found to be applicable to compound materials. It was corroborated that the anisotropy of SiC plays a significant role in the wettability of its surfaces; the contribution of the atomic surface termination was found to be a major parameter affecting wettability. Additionally, it was found that the calibration of the LJ parameters intrinsically includes the effects of the substrate structure. This was observed in the limit where the Si−O interaction was not considered and the contact angle was shown to be different from the pure graphitic surface. Finally, a contact angle reconciliation was found for the different crystallographic planes. The solid−liquid interaction energy per unit area served as reconciliation parameter, merging the calculated contact angle for different surfaces, which agrees with the results reported by Ramos-Alvarado el al.[43] However, this parameter did not reconcile the wetting behavior of the different atomic terminations.

AUTHOR INFORMATION

Corresponding Author

*E-mail: bzr52@engr.psu.edu.

ORCID

C. Ulises Gonzalez-Valle: 0000-0002-3683-4811

Bladimir Ramos-Alvarado: 0000-0003-2573-4134

Notes

The authors declare no competing financial interest.

ACKNOWLEDGMENTS

C. Ulises Gonzalez-Valle was partly supported by CONACyT (National Council on Science and Technology, Mexico) under the Mixed Scholarship Program.

REFERENCES

(1) Wang, X.; In, M.; Blanc, C.; Malgaretti, P.; Nobili, M.; Stocco, A. Wetting and Orientation of Catalytic Janus Colloids at the Surface of Water. *Faraday Discuss.* **2016**, *191*, 305−324.

DOI: 10.1021/acs.jpcc.7b12271
J. Phys. Chem. C 2018, 122, 7179−7186

(2) Niu, D.; Tang, G. H. The Effect of Surface Wettability on Water Vapor Condensation in Nanoscale. *Sci. Rep.* **2016**, *6*, No. 19192.
(3) Vo, T. Q.; Kim, B. Transport Phenomena of Water in Molecular Fluidic Channels. *Sci. Rep.* **2016**, *6*, No. 33881.
(4) Shavik, S. M.; Hasan, M. N.; Morshed, A. K. M. M.; Islam, M. Q. Molecular Dynamics Study of Effect of Different Wetting Conditions on Evaporation and Rapid Boiling of Ultra−Thin Argon Layer over Platinum Surface. *Procedia Eng.* **2015**, *105*, 446−451.
(5) Scocchi, G.; Sergi, D.; D'Angelo, C.; Ortona, A. Wetting and Contact-Line Effects for Spherical and Cylindrical Droplets on Graphene Layers: A Comparative Molecular-Dynamics Investigation. *Phys. Rev. E* **2011**, *84*, No. 061602.
(6) Kozbial, A.; Trouba, C.; Liu, H.; Li, L. Characterization of the Intrinsic Water Wettability of Graphite Using Contact Angle Measurements: Effect of Defects on Static and Dynamic Contact Angles. *Langmuir* **2017**, *33*, 959−967.
(7) Khalkhali, M.; Kazemi, N.; Zhang, H.; Liu, Q. Wetting at the Nanoscale: A Molecular Dynamics Study. *J. Chem. Phys.* **2017**, *146*, No. 114704.
(8) Werder, T.; Walther, J. H.; Jaffe, R. L.; Halicioglu, T.; Koumoutsakos, P. On the Water−Carbon Interaction for Use in Molecular Dynamics Simulations of Graphite and Carbon Nanotubes. *J. Phys. Chem. B* **2003**, *107*, 1345−1352.
(9) Taherian, F.; Marcon, V.; van der Vegt, N. F. A.; Leroy, F. What Is the Contact Angle of Water on Graphene? *Langmuir* **2013**, *29*, 1457−1465.
(10) Leroy, F.; Liu, S.; Zhang, J. Parametrizing Nonbonded Interactions from Wetting Experiments Via the Work of Adhesion: Example of Water on Graphene Surfaces. *J. Phys. Chem. C* **2015**, *119*, 28470−28481.
(11) Leroy, F.; Müller-Plathe, F. Dry-Surface Simulation Method for the Determination of the Work of Adhesion of Solid−Liquid Interfaces. *Langmuir* **2015**, *31*, 8335−8345.
(12) Erb, R. A. Wettability of Gold. *J. Phys. Chem.* **1968**, *72*, 2412−2417.
(13) Antony, A. C.; Liang, T.; Akhade, S. A.; Janik, M. J.; Phillpot, S. R.; Sinnott, S. B. Effect of Surface Chemistry on Water Interaction with Cu(111). *Langmuir* **2016**, *32*, 8061−8070.
(14) Barisik, M.; Beskok, A. Wetting Characterisation of Silicon (1,0,0) Surface. *Mol. Simul.* **2013**, *39*, 700−709.
(15) Ramos-Alvarado, B.; Kumar, S.; Peterson, G. P. Wettability of Graphitic-Carbon and Silicon Surfaces: Md Modeling and Theoretical Analysis. *J. Chem. Phys.* **2015**, *143*, No. 044703.
(16) Ramos-Alvarado, B.; Kumar, S.; Peterson, G. P. On the Wettability Transparency of Graphene-Coated Silicon Surfaces. *J. Chem. Phys.* **2016**, *144*, No. 014701.
(17) Ohler, B.; Langel, W. Molecular Dynamics Simulations on the Interface between Titanium Dioxide and Water Droplets: A New Model for the Contact Angle. *J. Phys. Chem. C* **2009**, *113*, 10189−10197.
(18) Köppen, S.; Langel, W. Simulation of the Interface of (100) Rutile with Aqueous Ionic Solution. *Surf. Sci.* **2006**, *600*, 2040−2050.
(19) Govind Rajan, A.; Sresht, V.; Pádua, A. A. H.; Strano, M. S.; Blankschtein, D. Dominance of Dispersion Interactions and Entropy over Electrostatics in Determining the Wettability and Friction of Two-Dimensional Mos2 Surfaces. *ACS Nano* **2016**, *10*, 9145−9155.
(20) Roccaforte, F.; Fiorenza, P.; Greco, G.; Vivona, M.; Lo Nigro, R.; Giannazzo, F.; Patti, A.; Saggio, M. Recent Advances on Dielectrics Technology for Sic and Gan Power Devices. *Appl. Surf. Sci.* **2014**, *301*, 9−18.
(21) Saddow, S. E. Silicon Carbide Materials for Biomedical Applications. In *Silicon Carbide Biotechnology*; Elsevier: Oxford, 2012; Chapter 1, pp 1−15.
(22) Oliveros, A.; Guiseppi-Elie, A.; Jaroszeski, M.; Saddow, S. E. Characterization of 3c-Sic (100) as a Platform for Detecting the Onset of Acute Myocardial Infarction (Ami). *MRS Proc.* **2012**, *1433*, No. 168.
(23) Ma, C.; Bai, S.; Peng, X.; Meng, Y. Improving Hydrophobicity of Laser Textured Sic Surface with Micro-Square Convexes. *Appl. Surf. Sci.* **2013**, *266*, 51−56.
(24) Mehregany, M.; Zorman, C. A.; Rajan, N.; Chien Hung, W. Silicon Carbide Mems for Harsh Environments. *Proc. IEEE* **1998**, *86*, 1594−1609.
(25) Mélinon, P.; Masenelli, B.; Tournus, F.; Perez, A. Playing with Carbon and Silicon at the Nanoscale. *Nat. Mater.* **2007**, *6*, 479−490.
(26) Shih, C.-J.; Wang, Q. H.; Lin, S.; Park, K.-C.; Jin, Z.; Strano, M. S.; Blankschtein, D. Breakdown in the Wetting Transparency of Graphene. *Phys. Rev. Lett.* **2012**, *109*, No. 176101.
(27) Israelachvili, J. N. Van Der Waals Forces between Particles and Surfaces. In *Intermolecular and Surface Forces*, 3rd ed.; Academic Press: Boston, 2011; Chapter 13, pp 253−289.
(28) Schravendijk, P.; van der Vegt, N. F. A. From Hydrophobic to Hydrophilic Solvation: An Application to Hydration of Benzene. *J. Chem. Theory Comput.* **2005**, *1*, 643−652.
(29) Aveyard, R.; Saleem, S. M. Work and Entropy of Adhesion at Liquid-Liquid Interfaces and the Relationship to Salt Desorption. *J. Chem. Soc., Faraday Trans. 1* **1977**, *73*, 896−904.
(30) Taherian, F.; Leroy, F.; van der Vegt, N. F. A. Interfacial Entropy of Water on Rigid Hydrophobic Surfaces. *Langmuir* **2013**, *29*, 9807−9813.
(31) Berendsen, H. J. C.; Grigera, J. R.; Straatsma, T. P. The Missing Term in Effective Pair Potentials. *J. Phys. Chem.* **1987**, *91*, 6269−6271.
(32) Ryckaert, J.-P.; Ciccotti, G.; Berendsen, H. J. C. Numerical Integration of the Cartesian Equations of Motion of a System with Constraints: Molecular Dynamics of N-Alkanes. *J. Comput. Phys.* **1977**, *23*, 327−341.
(33) Beckers, J. V. L.; Lowe, C. P.; De Leeuw, S. W. An Iterative ppm Method for Simulating Coulombic Systems on Distributed Memory Parallel Computers. *Mol. Simul.* **1998**, *20*, 369−383.
(34) Li, Z.; et al. Effect of Airborne Contaminants on the Wettability of Supported Graphene and Graphite. *Nat. Mater.* **2013**, *12*, 925−931.
(35) Plimpton, S. Fast Parallel Algorithms for Short-Range Molecular Dynamics. *J. Comput. Phys.* **1995**, *117*, 1−19.
(36) Humphrey, W.; Dalke, A.; Schulten, K. Vmd: Visual Molecular Dynamics. *J. Mol. Graphics* **1996**, *14*, 33−38.
(37) Hoover, W. G. Canonical Dynamics: Equilibrium Phase-Space Distributions. *Phys. Rev. A* **1985**, *31*, 1695−1697.
(38) Nosé, S. A Molecular Dynamics Method for Simulations in the Canonical Ensemble. *Mol. Phys.* **1984**, *52*, 255−268.
(39) Mazeau, K.; Rivet, A. Wetting the (110) and (100) Surfaces of Iβ Cellulose Studied by Molecular Dynamics. *Biomacromolecules* **2008**, *9*, 1352−1354.
(40) Grzelak, E. M.; Shen, V. K.; Errington, J. R. Molecular Simulation Study of Anisotropic Wetting. *Langmuir* **2010**, *26*, 8274−8281.
(41) Hashibon, A.; Adler, J.; Finnis, M. W.; Kaplan, W. D. Atomistic Study of Structural Correlations at a Liquid−Solid Interface. *Comput. Mater. Sci.* **2002**, *24*, 443−452.
(42) Godawat, R.; Jamadagni, S. N.; Garde, S. Characterizing Hydrophobicity of Interfaces by Using Cavity Formation, Solute Binding, and Water Correlations. *Proc. Natl. Acad. Sci. U.S.A.* **2009**, *106*, 15119−15124.
(43) Ramos-Alvarado, B.; Kumar, S.; Peterson, G. P. Solid−Liquid Thermal Transport and Its Relationship with Wettability and the Interfacial Liquid Structure. *J. Phys. Chem. Lett.* **2016**, *7*, 3497−3501.

DOI: 10.1021/acs.jpcc.7b12271
J. Phys. Chem. C 2018, 122, 7179−7186